Robotica: (2020) volume 38, pp. 550–563. © Cambridge University Press 2019
doi:10.1017/S0263574719000857

Hybrid-Trajectory Based Terminal Sliding Mode Control of a Flexible Space Manipulator with an Elastic Base

Xiaoyan Yu†,‡,*

†*School of Mechanical Engineering and Automation, Fuzhou University, Fuzhou, 350116 Fujian Province, China*
‡*Key Laboratory of Fluid Power and Intelligent Electro-Hydraulic Control (Fuzhou University), Fujian Province University, Fuzhou, 350116 Fujian Province, China*

(Accepted May 06, 2019. First published online: June 25, 2019)

SUMMARY
A hybrid-trajectory based terminal sliding mode controller (TSMC) is addressed for a free-flying two-flexible-link space manipulator with an elastic base. In this system, there are unknown but bounded external disturbances and parameters. First, the Lagrange dynamic model of the manipulator was established by the momentum conservation. Second, a TSMC based on desired trajectory was proposed, by which the terminal trajectories were asymptotically tracked and periodic flexible vibrations were excited. Then based on virtual control force, hybrid trajectories were generated, in which the flexible variables, the joint angular displacement errors and the base's attitude error were considered. Finally, a hybrid-trajectory TSMC was presented, by which the terminal trajectories were asymptotically tracked and the flexible vibrations were suppressed.

KEYWORDS: Flexible space manipulator; Elastic base; Terminal sliding mode control; Virtual control force; Hybrid trajectory; Flexible vibration suppression.

1. Introduction

Outer space is a significant field for the application of robotics technology. To assist astronauts in constructing and maintaining space modules and structures, robotic manipulators have been playing key roles in orbital operations.[1–5] To assure space robots' better tracking performances, various dynamic models and control techniques have been developed.[1–11] Most relevant works assumed that robot arms and the spacecraft are rigid.[6–11]

To reduce launch expenses and to prolong the orbit life, light space manipulators are needed. So, link structural flexibility is a well-known issue in the space manipulators.[12–18] Wu et al.[12] established the dynamic model of flexible dual-arm space manipulator, then made the inversion-dynamic nonlinear compensation and PD feedback to track the desired trajectory. Based on virtual rigid manipulator (VRM), Senda and Murotsu[13] proposed a methodology to propose stable manipulation-variable feedback controls of flexible space manipulators, this controller could accomplish positioning control and continuous path tracking control to a static target. To structurally flexible space-based manipulators, Carusone et al.[14] made an experiment of an end-effector trajectory tracking controller. Based on singular perturbation theory, various controllers[15–17] were proposed, with these controllers the desired trajectories can be asymptotically tracked and the vibrations of the flexible link of rigid-flexible free-floating space robot can be suppressed simultaneously. Furthermore, Yu and Chen[18] developed a composite singular perturbation adaptive controller, which is applicable to free-flying

* Corresponding author. E-mail: cool09@163.com

https://doi.org/10.1017/S0263574719000857 Published online by Cambridge University Press

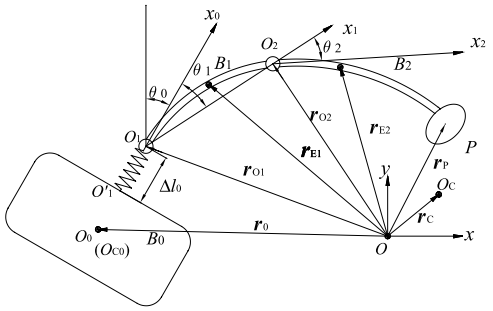


Fig. 1. Planar flexible space manipulator with an elastic base.

space manipulators with multiple flexible links. As the flexible vibrations are considered as a perturbation,[15–18] small deflection is assumed and the controllers may lose some robustness.

Overall, some studies on rigid space manipulators, rigid-flexible space manipulators or flexible space manipulators are made. But in all these works, the base is assumed to be rigid.[6–18] But in fact a spacecraft is not absolutely rigid.[19] Then motions of the space arms would disturb the position and the attitude of the base, and it also leads to vibrating motions on arms and the base. Meanwhile, vibrations of the base and the arms are cross-coupled and mutually excited. These disturbances are undesirable as it leads to a disturbed end-effector motion, and conventional control algorithms developed for terrestrial robots will not work in such a system.

The space manipulator dynamics is always involved with two kinds of uncertainties, which are structured uncertainty and unstructured uncertainty.[20] Sliding mode control (SMC) can ensure global stability and convergence of such space manipulator systems.[21–23] At the same time SMC is applicable to complex systems such as flexible manipulators due to its simplicity, effectiveness and robustness. The terminal sliding surfaces are proposed to assure the finite time stability[21,24–26] and terminal sliding mode controller (TSMC) is proposed. In this work, a TSMC was introduced to control a free-flying space manipulator with two flexible links and an elastic base. By this controller the terminal trajectories can be asymptotically tracked, but the flexible dynamics remained unstable. To stable the flexible dynamics, new desired trajectories were obtained based on the virtual control force. When the TSMC tracked the new generated desired trajectories, the flexible vibrations were stabilized effectively and good tracking performance was performed. The new desired trajectories, in which the flexible variables, the joint angular displacement errors and the base's attitude error were considered, are called the "hybrid" trajectories. Thus, the proposed control scheme is called the hybrid-trajectory control.

The paper is organized as follows. In Section 2, the dynamic model of a flexible space manipulator with an elastic base is formulated. In Section 3, a TSMC based on desired trajectory is proposed and its stability is verified by introducing the suitable Lyapunov function. In Section 4, a TSMC based on hybrid trajectory is introduced. In Section 5, experimental datum from a computer simulation by Matlab is presented. Finally, the conclusions are given in Section 6.

2. Dynamic Model of a Flexible Space Manipulator with an Elastic Base

In this section, first the kinematics analysis of a flexible space manipulator with an elastic base was made. Then the total energy associated with the manipulator system was computed using the kinematics formulations. Finally, the dynamic equations were derived by the Lagrange method.

A space manipulator with flexible links $B_i (i = 1, 2)$ and an elastic base B_0 is shown in Fig. 1. O_C is the mass center of the system, O_{C0} the mass center of the base and O_i the rotational center of the revolute joint between B_{i-1} and $B_i (i = 1, 2)$. θ_0 is the attitude angle of the base and θ_i is the ith link angular displacement $(i = 1, 2)$. $O_i - x_i y_i$ is the local right handed coordinate frame of $B_i (i = 0, 1, 2)$ and $O - xy$ is the inertial right handed coordinate frame. The elastic base was dynamically simplified as a rigid body with a constant stiffness k linear spring. The spring's elastic displacement is Δl_0.

In this manipulator, the same assumptions as those in ref.[18] were made. That is

(I) Each link was assumed to be long and slender. Therefore, transverse shear and the rotary inertia effects were negligible.

https://doi.org/10.1017/S0263574719000857 Published online by Cambridge University Press

(II) Links were considered to have constant cross-section and uniform material properties, that is, with constant mass density and Young's modulus, etc.
(III) External forces and torques were not applied to the system, and thus momentum conservation and equilibrium of forces strictly hold.
(IV) The motion of each joint was restricted to rotate in one degree of freedom, and its compliance and damping were ignored.
(VI) Each link had very small deflection.

Moreover, each actuator's mass center is the same as the center of the corresponding joint.

In the paper, $(\,)_{\mathrm{d}}$ is the desired variable of $(\,)$, $(\,)_{\mathrm{t}}$ the terminal variable of $(\,)$, $(\,)_{\mathrm{h}}$ the hybrid variable of $(\,)$, $\dot{(\,)}$ the first time derivative of $(\,)$, $\ddot{(\,)}$ the second time derivative of $(\,)$, $\mathbf{0}$ the zero matrix and I the identity matrix.

Based on the assumed mode method, the link bending deflections are refs.[18,27]

$$w_i\,(x_i,\,t) = \sum_{j=1}^{n_i} \varphi_{ij}\,(x_i)\,\delta_{ij}\,(t) \tag{1}$$

where $w_i\,(x_i,\,t)$ is the deflection of link B_i at $x_i (i = 1,\,2)$, $\varphi_{ij}\,(x_i)$ the shape function of mode j of link $B_i's$ deflection $(i = 1,\,2)$, $\delta_{ij}\,(t)$ the amplitude of mode j of link $B_i (i = 1,\,2)$ and $n_i (i = 1,\,2)$ the $B_i's$ number of modes. Here $n_i = 2$. In $(O - xy)$ frame, position vectors $\boldsymbol{r}_{Oi} (i = 1,\,2)$ of the center of the ith joint, position vectors $\boldsymbol{r}_{Ei} (i = 1,\,2)$ of arbitrary point E_i of link B_i and position vector $\boldsymbol{r}_P$ of the mass center of payload P are

$$\boldsymbol{r}_{\mathrm{O}i} = \boldsymbol{r}_0 + \Delta l_0 \boldsymbol{e}_{\mathrm{x}0} + \sum_{j=0}^{i-1} l_j \boldsymbol{e}_{\mathrm{x}j} \tag{2}$$

$$\boldsymbol{r}_{\mathrm{E}i} = \boldsymbol{r}_0 + \Delta l_0 \boldsymbol{e}_{\mathrm{x}0} + \sum_{j=0}^{i-1} l_j \boldsymbol{e}_{\mathrm{x}j} + x_i \boldsymbol{e}_{\mathrm{x}i} - w_i\,(x_i,\,t)\,\boldsymbol{e}_{\mathrm{y}i} \tag{3}$$

$$\boldsymbol{r}_{\mathrm{P}} = \boldsymbol{r}_0 + \Delta l_0 \boldsymbol{e}_{\mathrm{x}0} + \sum_{j=0}^{2} l_j \boldsymbol{e}_{\mathrm{x}j} - w_2\,(l_2,\,t)\,\boldsymbol{e}_{\mathrm{y}2} \tag{4}$$

where $\boldsymbol{r}_0$ is the position vector of the mass center O_{C0} of B_0 in $(O - xy)$ frame, l_0 the distance between point O and O_1', li the length of B_i along the x_i axis $(i = 1,\,2)$, $\boldsymbol{e}_{xi} (i = 1,\,2)$ the unit vector along the x_i axis in $(O - xy)$ frame and $\boldsymbol{e}_{yi} (i = 1,\,2)$ the unit vector along the y_i axis in $(O - xy)$ frame.

Therefore, position vector $\boldsymbol{r}_{\mathrm{C}}$ of the mass center O_{C} of the entire system in $(O - xy)$ frame is

$$\boldsymbol{r}_{\mathrm{C}} = \frac{m_0\,\boldsymbol{r}_0 + m_{\mathrm{P}}\,\boldsymbol{r}_{\mathrm{P}} + \sum_{i=1}^{2}\left(\rho_i \int_0^{l_i} \boldsymbol{r}_{\mathrm{E}i} d_{x_i} + m_{\mathrm{a}i}\,\boldsymbol{r}_{\mathrm{O}i}\right)}{M} \tag{5}$$

where m_i is the mass of $B_i (i = 0,\,1,\,2)$, m_P the mass of payload P, m_{ai} the mass of the ith actuator $(i = 1,\,2)$, ρ_i the uniform density of the flexible link $B_i (i = 1,\,2)$ and $M = m_0 + \sum_{i=1}^{2}\left(\int_0^{l_i} \rho_i d_{x_i} + m_{\mathrm{a}i}\right) + m_{\mathrm{P}}$ the total mass of the system. So, $\boldsymbol{r}_0$ and $\boldsymbol{r}_{Oi}, \boldsymbol{r}_{Ei} (i = 1,\,2)$ and $\boldsymbol{r}_P$ are expressed with $\boldsymbol{r}_C$

$$\boldsymbol{r}_0 = \boldsymbol{r}_{\mathrm{C}} + \sum_{k=0}^{2} N_{\mathrm{x}k} \boldsymbol{e}_{xk} + \sum_{k=1}^{2}\left(\sum_{j=1}^{n_k} N_{ykj}\delta_{kj}\right)\boldsymbol{e}_{yk} \tag{6}$$

$$\boldsymbol{r}_{\mathrm{O}i} = \boldsymbol{r}_{\mathrm{C}} + \sum_{k=0}^{2} N_{\mathrm{x}k} \boldsymbol{e}_{\mathrm{x}k} + \sum_{k=1}^{2}\left(\sum_{j=1}^{\mathrm{n}_k} N_{ykj}\delta_{kj}\right)\boldsymbol{e}_{\mathrm{y}k} + \sum_{k=0}^{i-1} l_k \boldsymbol{e}_{\mathrm{x}k} \tag{7}$$

$$\boldsymbol{r}_{\mathrm{E}i} = \boldsymbol{r}_{\mathrm{C}} + \sum_{k=0}^{2} N_{\mathrm{x}k} \boldsymbol{e}_{\mathrm{x}k} + \sum_{k=1}^{2}\left(\sum_{j=1}^{\mathrm{n}_k} N_{ykj}\delta_{kj}\right)\boldsymbol{e}_{\mathrm{y}k} + \sum_{k=0}^{i-1} l_k \boldsymbol{e}_{\mathrm{x}k} + x_i \boldsymbol{e}_{\mathrm{x}i} - w_i\,(x_i,\,t)\,\boldsymbol{e}_{\mathrm{y}i} \tag{8}$$

https://doi.org/10.1017/S0263574719000857 Published online by Cambridge University Press

$$r_{\mathrm{P}} = r_{\mathrm{C}} + \sum_{k=0}^{2} N_{\mathrm{x}k} e_{xk} + \sum_{k=1}^{2} \left(\sum_{j=1}^{n_k} N_{ykj} \delta_{kj} \right) e_{yk} + \sum_{k=0}^{2} l_k e_{xk} - w_2 \left(l_2, t \right) e_{y2} \tag{9}$$

where $N_{\mathrm{x}k}(k = 0, 1, 2)$, $N_{ykj}(k = 0, 1, 2; j = 1, 2)$ are the functions of m_0, $\rho_i(i = 1, 2)$, $m_{ai}(i = 1, 2)$, m_P and $l_i(i = 0, 1, 2)$. Differentiating Eqs. (6)–(9) with respect to time t, velocity vector $\dot{\boldsymbol{r}}_0$, $\dot{\boldsymbol{r}}_{\mathrm{O}i}$, $\dot{\boldsymbol{r}}_{\mathrm{E}i}$ $(i = 1, 2)$ and $\dot{\boldsymbol{r}}_{\mathrm{P}}$ can be derived. Then the manipulator's kinetic energy is

$$T = T_0 + \sum_{\mathrm{i}=1}^{2} \left(\mathrm{T}_i + T_{ai} \right) + \mathrm{T}_P \tag{10}$$

where T_i is the kinetic energy of $B_i(i = 0, 1, 2)$, $T_{\mathrm{a}i}$ the kinetic energy of the ith actuator $(i = 1, 2)$, T_P the kinetic energy of payload P, $T_0 = \frac{1}{2}(m_0 \dot{r}_0^2 + I_0 \dot{\theta}_0^2)$, $T_i = \frac{1}{2}\rho_i \int_0^{l_i} \dot{r}_{\mathrm{E}i}^2 d_{x_i}$, $T_{\mathrm{a}i} = \frac{1}{2}\left(m_{\mathrm{a}i} \dot{r}_{Oi}^2 + I_{ai} \left(\left(\sum_{k=0}^{i} \dot{\theta}_k \right) \right)^2 \right)$ $T_{\mathrm{P}} = \frac{1}{2}(m_{\mathrm{P}} \dot{r}_P^2 + I_P (\sum_{k=0}^{2} \dot{\theta}_k + \dot{\alpha}_{2l})^2)$; $\dot{\alpha}_{2\mathrm{l}} = \sum_{k=1}^{\mathrm{n}_2} (\varphi'_{2k}(l_2) \dot{\delta}_{2k}(t))$, $\varphi'_{2k}(l_2) = (\frac{d\varphi_{2k}(x_2)}{dx_2})_{x_2 = l_2}$, I_0 the inertial moment of B_0 with respect to its mass center, I_{ai} the inertial moment of the ith actuator $(i = 1, 2)$ with respect to its mass center and I_P is the inertial moment of payload P with respect to its mass center.

Ignoring the microgravity, the manipulator's potential energy is

$$V = \frac{1}{2} \left(\sum_{i=1}^{2} \left((EI)_i \int_0^{l_i} \left(\frac{\partial^2 w_i \left(x_i, t \right)}{\partial^2 x_i} \right)^2 d_{x_i} \right) + k \left(\Delta l_0 \right)^2 \right) \tag{11}$$

where $(EI)_i$ is the flexural rigidity of link $B_i(i = 1, 2)$.

The manipulator dynamic equation is derived as ref.[28]

$$\mathbf{D}(\boldsymbol{q})\ddot{\boldsymbol{q}} + \mathbf{H}(\boldsymbol{q}, \dot{\boldsymbol{q}})\dot{\boldsymbol{q}} + \mathbf{K}\boldsymbol{q} = \left[\boldsymbol{\tau}^{\mathrm{T}} \; 0^{\mathrm{T}} \right]^{\mathrm{T}} \tag{12}$$

where $\boldsymbol{q} = [\boldsymbol{q}_{\mathrm{r}}^{\mathrm{T}} \; \boldsymbol{q}_{\mathrm{f}}^{\mathrm{T}}]^{\mathrm{T}} \in \mathbf{R}^{8\times 1}$ denotes the generalized coordinate, $\boldsymbol{q}_{\mathrm{f}} = [\Delta l_0 \; \delta_{11} \; \delta_{12} \; \delta_{21} \; \delta_{22}]^T \in \mathbf{R}^{5\times 1}$, $\boldsymbol{q}_{\mathrm{r}} = [\theta_0 \; \theta_1 \; \theta_2]^T \in \mathbf{R}^{3\times 1}$ and $\boldsymbol{\tau} = [\tau_0 \; \tau_1 \; \tau_2]^T \in \mathbf{R}^{3\times 1}$ denote the input torques. $\mathbf{D}(\boldsymbol{q})$ denotes the 8×8 inertia matrix, $\mathbf{H}(\boldsymbol{q}, \dot{\boldsymbol{q}})\dot{\boldsymbol{q}}$ denotes the 8-dimensional vector of the Coriolis and centrifugal forces, $\mathbf{K} = \mathrm{diag}([\mathbf{0}, \mathbf{K}_{\mathrm{f}}])$, $\mathbf{K}_{\mathrm{f}} \in \mathrm{R}^{5\times 5}$ is the stiffness matrix.

3. Terminal Sliding Mode Controller Based on Desired Trajectory

By proposing a dynamic, nonlinear sliding surface, the TSMC can guarantee the system's stability and track the desired state in finite time.[29] In this section, firstly a sliding surface was proposed, then a TSMC based on this sliding surface was presented. The desired trajectories were generated from the terminal trajectories by a second order command generator. This TSMC can ensure the good tracking performance, but cannot suppress the flexible vibrations perfectly.

By partitioned matrix, Eq. (12) is rewritten as

$$\begin{bmatrix} \mathbf{D}_{\mathrm{rr}} & \mathbf{D}_{\mathrm{rf}} \\ \mathbf{D}_{\mathrm{fr}} & \mathbf{D}_{\mathrm{ff}} \end{bmatrix} \begin{bmatrix} \ddot{\boldsymbol{q}}_{\mathrm{r}} \\ \ddot{\boldsymbol{q}}_{\mathrm{f}} \end{bmatrix} + \begin{bmatrix} \mathbf{H}_{\mathrm{rr}} & \mathbf{H}_{\mathrm{rf}} \\ \mathbf{H}_{\mathrm{fr}} & \mathbf{H}_{\mathrm{ff}} \end{bmatrix} \begin{bmatrix} \dot{\boldsymbol{q}}_{\mathrm{r}} \\ \dot{\boldsymbol{q}}_{\mathrm{f}} \end{bmatrix} + \begin{bmatrix} \mathbf{0} \\ \mathbf{K}_{\mathrm{f}} \boldsymbol{q}_{\mathrm{f}} \end{bmatrix} = \begin{bmatrix} \boldsymbol{\tau} \\ \mathbf{0} \end{bmatrix} \tag{13}$$

where $\mathbf{D}_{\mathrm{rr}} \in \mathbf{R}^{3\times 3}$, $\mathbf{D}_{\mathrm{rf}} = \mathbf{D}_{\mathrm{fr}}^{\mathrm{T}} \in \mathbf{R}^{3\times 5}$ and $\mathbf{D}_{\mathrm{ff}} \in \mathbf{R}^{5\times 5}$, $\mathbf{H}_{\mathrm{rr}} \in \mathbf{R}^{3\times 3}$, $\mathbf{H}_{\mathrm{rf}} = \mathbf{H}_{\mathrm{fr}}^{\mathrm{T}} \in \mathbf{R}^{3\times 5}$ and $\mathbf{H}_{\mathrm{ff}} \in \mathbf{R}^{5\times 5}$.

So Eq. (13) is transformed into

$$\mathbf{D}_{\mathrm{rr}}\ddot{\boldsymbol{q}}_{\mathrm{r}} + \mathbf{D}_{\mathrm{rf}}\ddot{\boldsymbol{q}}_{\mathrm{f}} + \mathbf{H}_{\mathrm{rr}}\dot{\boldsymbol{q}}_{\mathrm{r}} + \mathbf{H}_{\mathrm{rf}}\dot{\boldsymbol{q}}_{\mathrm{f}} = \boldsymbol{\tau} \tag{14}$$

$$\mathbf{D}_{\mathrm{fr}}\ddot{\boldsymbol{q}}_{\mathrm{r}} + \mathbf{D}_{\mathrm{ff}}\ddot{\boldsymbol{q}}_{\mathrm{f}} + \mathbf{H}_{\mathrm{fr}}\dot{\boldsymbol{q}}_{\mathrm{r}} + \mathbf{H}_{\mathrm{ff}}\dot{\boldsymbol{q}}_{\mathrm{f}} + \mathbf{K}_{\mathrm{f}}\boldsymbol{q}_{\mathrm{f}} = \mathbf{0} \tag{15}$$

Since $\mathbf{D}_{\mathrm{ff}}$ is symmetric and positive definite, then Eq. (16) is derived

$$\ddot{\boldsymbol{q}}_{\mathrm{f}} = -\mathbf{D}_{\mathrm{ff}}^{-1} \left(\mathbf{D}_{\mathrm{fr}}\ddot{\boldsymbol{q}}_{\mathrm{r}} + \mathbf{H}_{\mathrm{fr}}\dot{\boldsymbol{q}}_{\mathrm{r}} + \mathbf{H}_{\mathrm{ff}}\dot{\boldsymbol{q}}_{\mathrm{f}} + \mathbf{K}_{\mathrm{f}}\boldsymbol{q}_{\mathrm{f}} \right) \tag{16}$$

https://doi.org/10.1017/S0263574719000857 Published online by Cambridge University Press

Substituting Eq. (16) into Eq. (14), the manipulator dynamic equation is given by

$$\mathbf{D}\ddot{\boldsymbol{q}}_{\mathrm{r}} + \boldsymbol{h} = \boldsymbol{\tau} \tag{17}$$

where $\mathbf{D} = \mathbf{D}_{\mathrm{rr}} - \mathbf{D}_{\mathrm{rf}}\mathbf{D}_{\mathrm{ff}}^{-1}\boldsymbol{D}_{\mathrm{fr}}$, $\boldsymbol{h} = \mathbf{H}_{\mathrm{rr}}\dot{\boldsymbol{q}}_{\mathrm{r}} + \mathbf{H}_{\mathrm{rf}}\dot{\boldsymbol{q}}_{\mathrm{f}} - \mathbf{D}_{\mathrm{rf}}\mathbf{D}_{\mathrm{ff}}^{-1}\left(\mathbf{H}_{\mathrm{fr}}\dot{\boldsymbol{q}}_{\mathrm{r}} + \mathbf{H}_{\mathrm{ff}}\dot{\boldsymbol{q}}_{\mathrm{f}} + \mathbf{K}_{\mathrm{f}}\boldsymbol{q}_{\mathrm{f}}\right)$.

Obviously $\mathbf{D}$ is symmetric and positive definite, so it is invertible. Introduce the state vector $\boldsymbol{x}_1 = \boldsymbol{q}_{\mathrm{r}}$, $\dot{\boldsymbol{x}}_1 = \boldsymbol{x}_2 = \dot{\boldsymbol{q}}_{\mathrm{r}}$, the dynamic Eq. (17) is expressed as

$$\begin{cases} \dot{\boldsymbol{x}}_1 = \boldsymbol{x}_2 \\ \dot{\boldsymbol{x}}_2 = \mathbf{D}^{-1}\left(\boldsymbol{\tau} - \boldsymbol{h}\right) \end{cases} \tag{18}$$

Additional disturbances $\boldsymbol{\tau}_{\mathrm{d}}$ is considered, then

$$\begin{cases} \dot{\boldsymbol{x}}_1 = \boldsymbol{x}_2 \\ \dot{\boldsymbol{x}}_2 = \mathbf{D}^{-1}\left(\boldsymbol{\tau} + \boldsymbol{\tau}_{\mathrm{d}} - \boldsymbol{h}\right) \end{cases} \tag{19}$$

Define an output displacement error vector $\boldsymbol{e}$

$$\boldsymbol{e} = \boldsymbol{x}_{1\mathrm{d}} - \boldsymbol{x}_1 \tag{20}$$

Then the output velocity error $\dot{e}$ is

$$\dot{\boldsymbol{e}} = \boldsymbol{x}_{2\mathrm{d}} - \boldsymbol{x}_2 \tag{21}$$

where $\boldsymbol{x}_{1\mathrm{d}}$ and $\boldsymbol{x}_{2\mathrm{d}}$ are the desired displacements and desired velocities, respectively.

The following sliding surface is presented

$$\boldsymbol{s}\left(t\right) = \mathbf{Z}\left[\boldsymbol{e}^{\mathrm{T}}\ \dot{\boldsymbol{e}}^{\mathrm{T}}\right]^{\mathrm{T}} - \mathbf{Z}\left[\boldsymbol{p}^{\mathrm{T}}\left(t\right)\dot{\boldsymbol{p}}^{\mathrm{T}}\left(t\right)\right]^{\mathrm{T}} \tag{22}$$

where $\mathbf{Z} = [\mathbf{Z}_1\ \ \mathbf{Z}_2]$, $\mathbf{Z}_i = diag(z_i^0, z_i^1, z_i^2)(i = 1, 2)$, $z_i^j(i = 1, 2; j = 0, 1, 2)$ are positive constants, $p\left(t\right) = [p_0\left(t\right)\ p_1\left(t\right)\ \ p_2\left(t\right)]^{\mathrm{T}}$ and $p_j\left(t\right)(j = 0, 1, 2)$ satisfy the following assumptions.

Assumption 1. *$p_j\left(t\right) : \mathbf{R}^+ \to \mathbf{R}$, $p_j\left(t\right) \in C^2[0, \infty)$, $\dot{p}_j\left(t\right) \in L^\infty$, $\ddot{p}_j\left(t\right) \in L^\infty$. To any positive constant T, $p_j\left(t\right)$ is bounded while $t \in [0, T]$. At the same time, $p_j\left(0\right) = e_j\left(0\right)$, $\dot{p}_j\left(0\right) = \dot{e}_j\left(0\right)$, $\ddot{p}_j\left(t\right) = \ddot{e}_j\left(0\right)$.*

Introduce the Lyapunov function

$$V = \frac{\boldsymbol{s}^{\mathrm{T}}\boldsymbol{s}}{2} \tag{23}$$

The derivative of the V is

$$\begin{aligned} \dot{V} &= \boldsymbol{s}^{\mathrm{T}}\dot{\boldsymbol{s}} \\ &= \boldsymbol{s}^{\mathrm{T}}\left(\mathbf{Z}_1\left(\dot{\boldsymbol{e}} - \dot{\boldsymbol{p}}\left(t\right)\right) + \mathbf{Z}_2\left(\dot{\boldsymbol{x}}_2 - \boldsymbol{x}_{2\mathbf{d}} - \ddot{\boldsymbol{p}}\left(t\right)\right)\right) \\ &= \boldsymbol{s}^{\mathrm{T}}\left(\mathbf{Z}_1\left(\dot{\boldsymbol{e}} - \dot{\boldsymbol{p}}\left(t\right)\right) + \mathbf{Z}_2\left(\mathbf{D}^{-1}\left(\boldsymbol{\tau} + \boldsymbol{\tau}_{\mathrm{d}} - \boldsymbol{h}\right) - \boldsymbol{x}_{2\mathrm{d}} - \ddot{\boldsymbol{p}}\left(t\right)\right)\right) \end{aligned} \tag{24}$$

Suppose random disturbance $\left|\boldsymbol{\tau}_{\mathrm{d}j}\right| \le c_{\mathrm{d}j}\ (j = 1, \ldots, k)$ where $c_{\mathrm{d}j}$ are known positive constants. The following SMC is proposed

$$\boldsymbol{\tau} = \mathbf{D}\left(\mathbf{Z}_2^{-1}\mathbf{Z}_1\left(\dot{\boldsymbol{p}}\left(t\right) - \dot{\boldsymbol{e}}\right) + \boldsymbol{x}_{2d} + \ddot{\boldsymbol{p}}\left(t\right)\right) - \mathbf{D}\frac{\mathbf{Z}_2^{\mathrm{T}}\boldsymbol{s}}{\left\|\mathbf{Z}_2^{\mathrm{T}}\boldsymbol{s}\right\|}\left(\left\|\mathbf{D}^{-1}\boldsymbol{c}_{\mathrm{d}}\right\| + c\right) + \boldsymbol{h} \tag{25}$$

where $\boldsymbol{c}_{\mathrm{d}} = [c_{\mathrm{d}1} \cdots c_{\mathrm{d}j} \cdots c_{\mathrm{d}k}]^{\mathrm{T}}$ and c is a positive constant.

$$\dot{V} \le \left\|\boldsymbol{s}^{\mathrm{T}}\mathbf{Z}_2\right\|\left\|\mathbf{D}^{-1}\boldsymbol{\tau}_{\mathrm{d}}\right\| - \boldsymbol{s}^{\mathrm{T}}\mathbf{Z}_2\frac{\mathbf{Z}_2^{\mathrm{T}}\boldsymbol{s}}{\left\|\mathbf{Z}_2^{\mathrm{T}}\boldsymbol{s}\right\|}\left(\left\|\mathbf{D}^{-1}\boldsymbol{c}_{\mathrm{d}}\right\| + c\right) \tag{26}$$

Obviously $\dot{V} \le 0$, so $\lim_{t\to\infty} \boldsymbol{s} = \mathbf{0}$.

By assumption 1, $\boldsymbol{s}\left(0\right)$ is

$$\boldsymbol{s}\left(0\right) = \boldsymbol{Z}\left(\begin{bmatrix} \boldsymbol{e}\left(0\right) \\ \dot{\boldsymbol{e}}\left(0\right) \end{bmatrix} - \begin{bmatrix} \boldsymbol{p}\left(0\right) \\ \dot{\boldsymbol{p}}\left(0\right) \end{bmatrix}\right) = \mathbf{0} \tag{27}$$

https://doi.org/10.1017/S0263574719000857 Published online by Cambridge University Press

Since $\boldsymbol{s}$ (0) is zero, the arbitrary initial state is on the sliding surface. Compared to the ordinary SMC there are no reaching phases for this SMC, so this SMC ensures the system's dynamics Eq. (19) is globally robust and stable. So, $\boldsymbol{s}(t) = \mathbf{0}$ and $[\boldsymbol{e}^{\mathrm{T}}(t)\dot{\boldsymbol{e}}^{\mathrm{T}}(t)]^{\mathrm{T}} = [\boldsymbol{p}^{\mathrm{T}}(t)\dot{\boldsymbol{p}}^{\mathrm{T}}(t)]^{\mathrm{T}}$. Define appropriate $\boldsymbol{p}$ to ensure $\boldsymbol{p}(t) \equiv \mathbf{0}$ and $\dot{\boldsymbol{p}}(t) \equiv \mathbf{0}$ for all $t \geq T$. Then $\boldsymbol{e}(t) \equiv \mathbf{0}$ and $\dot{\boldsymbol{e}}(t) \equiv \mathbf{0}$ for all $t \geq T$. So, the tracking error $\boldsymbol{e}$ and $\dot{\boldsymbol{e}}$ of the system Eq. (19) converge to 0 in finite time T. By assumption 1, $p_j(t)$ is defined as

$$p_j(t) = \begin{cases} \sum_{k=0}^{5} c_{jk} t^k & 0 \leq t \leq T \\ 0 & t > T \end{cases} \tag{28}$$

where $c_{j3} = \frac{a_{00}}{T^3} e_j(0) + \frac{a_{01}}{T^2}\dot{e}_j(0) + \frac{a_{02}}{T}\ddot{e}_j(0)$, $c_{j4} = \frac{a_{10}}{T^4} e_j(0) + \frac{a_{11}}{T^3}\dot{e}_j(0) + \frac{a_{12}}{T^2}\ddot{e}_j(0)$, $c_{j5} = \frac{a_{20}}{T^5} e_j(0) + \frac{a_{21}}{T^4}\dot{e}_j(0) + \frac{a_{22}}{T^3}\ddot{e}_j(0)$, c_{j0}, c_{j1}, c_{j2} and a_{hl} $(h, l = 0, 1, 2)$ are defined later.

Then the first and the second derivative of $p_j(t)$ are

$$\dot{p}_j(t) = \begin{cases} \sum_{k=1}^{5} k c_{jk} t^{k-1} & 0 \leq t \leq T \\ 0 & t > T \end{cases} \tag{29}$$

$$\ddot{p}_j(t) = \begin{cases} \sum_{k=2}^{5} k(k-1) c_{jk} t^{k-2} & 0 \leq t \leq T \\ 0 & t > T \end{cases} \tag{30}$$

Since $p_j(0) = e_j(0)$, $\dot{p}_j(0) = \dot{e}_j(0)$, $\ddot{p}_j(0) = \ddot{e}_j(0)$, the $c_{j0} = e_j(0)$, $c_{j1} = \dot{e}_j(0)$, $c_{j2} = 0.5\ddot{e}_j(0)$. To ensure $p_j(T) = 0$, $\dot{p}_j(T) = 0$, $p_j(T) = 0$, a_{hl} $(h, l = 0, 1, 2)$, then

$$\begin{cases} a_{00} + a_{10} + a_{20} = -1 \\ 3a_{00} + 4a_{10} + 5a_{20} = 0 \\ 6a_{00} + 12a_{10} + 20a_{20} = 0 \end{cases} \tag{31}$$

$$\begin{cases} a_{01} + a_{11} + a_{21} = -1 \\ 3a_{01} + 4a_{11} + 5a_{21} = -1 \\ 6a_{01} + 12a_{11} + 20a_{21} = 0 \end{cases} \tag{32}$$

$$\begin{cases} a_{02} + a_{12} + a_{22} = -0.5 \\ 3a_{02} + 4a_{12} + 5a_{22} = -1 \\ 6a_{02} + 12a_{12} + 20a_{22} = -1 \end{cases} \tag{33}$$

where a_{hl} $(h, l = 0, 1, 2)$ are solved out as $a_{00} = -10$, $a_{10} = 15$, $a_{20} = -6$, $a_{01} = -6$, $a_{11} = 8$, $a_{21} = -3$, $a_{02} = -1.5$, $a_{12} = 1.5$, $a_{22} = -0.5$.

$\frac{1}{\|\mathbf{Z}_2^{\mathrm{T}} s\|}\mathbf{Z}_2^{\mathrm{T}}\boldsymbol{s}$ is discontinuous, which leads to trajectory chattering around the sliding surface $\boldsymbol{s} = \mathbf{0}$. To avoid the above trajectory chattering the following continuous function vector is defined to replace $\frac{1}{\|\mathbf{Z}_2^{\mathrm{T}} s\|}\mathbf{Z}_2^{\mathrm{T}}\boldsymbol{s}$.

$$f(s) = \frac{\mathbf{Z}^{\mathrm{T}}\boldsymbol{s}}{\left\|\mathrm{Z}^{\mathrm{T}}\boldsymbol{s}\right\| + (c_0 + c_1 \|\boldsymbol{e}\|)} \tag{34}$$

where c_0 and c_1 are positive constants.

During the orbit manipulation of space manipulator, the terminal vector $\boldsymbol{q}_{\mathrm{t}}$ is often known. The desired trajectory $\boldsymbol{x}_{1\mathrm{d}}$ is obtained by

$$\ddot{\boldsymbol{x}}_{1\mathrm{d}} + \mathbf{K}_1\dot{\boldsymbol{x}}_{\mathbf{1d}} + \mathbf{K}_2\boldsymbol{x}_{\mathbf{1d}} = \mathbf{K}_2\boldsymbol{q}_{\mathbf{t}} \tag{35}$$

where $\mathbf{K}_1 = \mathrm{diag}([2\zeta_0\omega_0, 2\zeta_1\omega_1, 2\zeta_2\omega_2])$, $\mathbf{K}_2 = \mathrm{diag}([\omega_0^2, \omega_1^2, \omega_2^2])$, $\zeta_i > 0$, $\omega_i > 0$ $(i = 0, 1, 2)$. $\boldsymbol{q}_{\mathrm{t}} = [\theta_{0\mathrm{t}}\ \theta_{1\mathrm{t}}\ \theta_{2\mathrm{t}}]^{\mathrm{T}}$.

The operational control strategy of the proposed TSMC based on desired trajectory is shown in Fig. 2.

https://doi.org/10.1017/S0263574719000857 Published online by Cambridge University Press

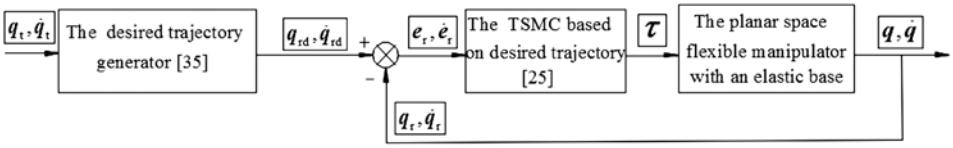


Fig. 2. The operational control strategy of the proposed TSMC based on desired trajectory.

By the controller Eq. (25) the terminal trajectories are asymptotically tracked, nevertheless, the link flexible vibrations and the elastic base deformation are excited. In the next section based on the virtual control force, a hybrid trajectory TSMC is proposed. By this hybrid trajectory TSMC the terminal trajectories can be asymptotically tracked while the flexible vibrations can be suppressed.

4. Terminal Sliding Mode Controller Based on Hybrid Trajectory

In this section, a new hybrid trajectory was generated based on the virtual control force concept and the terminal trajectory. The virtual control force played an important role in generating a new desired trajectory to stabilize the flexible vibrations. The new desired trajectory, which reflects the flexible variables as well as the base's attitude, the joint angles, is referred to as the "hybrid" trajectory. Thus, the proposed control scheme is called the "hybrid" control scheme.

Define error vector $\boldsymbol{e}_{\mathrm{h}}$

$$\boldsymbol{e}_{\mathrm{h}} = \boldsymbol{x}_{\mathrm{h}} - \boldsymbol{q}_{\mathrm{t}} \tag{36}$$

where $\boldsymbol{x}_{\mathrm{h}}$ is the hybrid trajectory. The hybrid trajectory $\boldsymbol{x}_{\mathrm{h}}$ is obtained by

$$\begin{cases} \boldsymbol{x}_{\mathrm{h}} = \boldsymbol{q}_{\mathrm{t}} + \boldsymbol{e}_{\mathrm{h}} \\ \ddot{\boldsymbol{e}}_{\mathrm{h}} + \mathbf{K}_1 \dot{\boldsymbol{e}}_{\mathbf{h}} + \mathbf{K}_2 \boldsymbol{e}_{\mathbf{h}} = \boldsymbol{f} \end{cases} \tag{37}$$

where vector $\boldsymbol{f}$ denotes the virtual control force. $\boldsymbol{f}$ is defined later. Then the controller based on hybrid trajectory is

$$\boldsymbol{\tau} = \mathbf{D}\left(\mathbf{Z}_2^{-1}\mathbf{Z}_1\left(\dot{\boldsymbol{p}}\left(t\right) - \dot{\boldsymbol{e}}_{\mathrm{rh}}\right) + \boldsymbol{x}_{2\mathrm{d}} + \ddot{\boldsymbol{p}}\left(t\right)\right) - \mathbf{D}\frac{\mathbf{Z}_2^{\mathrm{T}}\boldsymbol{s}_{\mathrm{rh}}}{\left\|\mathbf{Z}_2^{\mathrm{T}}\boldsymbol{s}_{\mathrm{rh}}\right\|}\left(\left\|\mathbf{D}^{-1}\boldsymbol{c}_{\mathrm{d}}\right\| + c\right) + \boldsymbol{h} \tag{38}$$

where $\boldsymbol{x}_{1\mathrm{d}} = \boldsymbol{x}_{\mathrm{h}}$, $\boldsymbol{x}_{2\mathrm{d}} = \dot{\boldsymbol{x}}_{1\mathrm{d}} = \dot{\boldsymbol{x}}_{\mathrm{h}}$, $\ddot{\boldsymbol{x}}_{1\mathrm{d}} = \ddot{\boldsymbol{x}}_{\mathrm{h}}$, $\boldsymbol{s}_{\mathrm{rh}} = \mathbf{Z}[\boldsymbol{e}_{\mathrm{rh}}^{\mathrm{T}}\ \dot{\boldsymbol{e}}_{\mathrm{rh}}^{\mathrm{T}}]^{\mathrm{T}} - \mathbf{Z}[\boldsymbol{p}^{\mathrm{T}}\left(t\right)\ \dot{\boldsymbol{p}}^{\mathrm{T}}\left(t\right)]^{\mathrm{T}}$, $\boldsymbol{e}_{\mathrm{rh}} = \boldsymbol{x}_1 - \boldsymbol{x}_{\mathrm{h}}$, $\dot{\boldsymbol{e}}_{\mathrm{rh}} = \boldsymbol{x}_2 - \dot{\boldsymbol{q}}_{\mathrm{h}}$; $\boldsymbol{p}\left(t\right) = [p_0\left(t\right)\ \ p_1\left(t\right)\ \ p_2\left(t\right)]^{\mathrm{T}}$, $\dot{\boldsymbol{p}}\left(t\right) = [\dot{p}_0\left(t\right)\ \dot{p}_1\left(t\right)\ \ \dot{\boldsymbol{p}}_2\left(t\right)]^{\mathrm{T}}$, $\ddot{\boldsymbol{p}}\left(t\right) = [\ddot{p}_0\left(t\right)\ \ \ddot{p}_1\left(t\right)\ \ \ddot{p}_2\left(t\right)]^{\mathrm{T}}$, $p_j\left(t\right)$, $\dot{p}_j\left(t\right)$ and $\ddot{p}_j\left(t\right)(j = 0, 1, 2)$ are the same as Eqs. (28), (29) and (30), where $c_{j0} = e_{\mathrm{rh}j}(0)$, $c_{j1} = \dot{e}_{\mathrm{rh}j}(0)$, $c_{j2} = 0.5\ddot{e}_{\mathrm{rh}j}(0)$, $c_{j3} = \frac{a_{00}}{T^3}e_{\mathrm{rh}j}(0) + \frac{a_{01}}{T^2}\dot{e}_{\mathrm{rh}j}(0) + \frac{a_{02}}{T}\ddot{e}_{\mathrm{rh}j}(0)$, $c_{j4} = \frac{a_{10}}{T^4}e_{\mathrm{rh}j}(0) + \frac{a_{11}}{T^3}\dot{e}_{\mathrm{rh}j}(0) + \frac{a_{12}}{T^2}\ddot{e}_{\mathrm{rh}j}(0)$, $c_{j5} = \frac{a_{20}}{T^5}e_{\mathrm{rh}j}(0) + \frac{a_{21}}{T^4}\dot{e}_{\mathrm{rh}j}(0) + \frac{a_{22}}{T^3}\ddot{e}_{\mathrm{rh}j}(0)$.

So, the system actual error $\boldsymbol{e}_{\mathrm{t}} = \boldsymbol{x}_1 - \boldsymbol{q}_{\mathrm{t}} = \boldsymbol{q}_{\mathrm{r}} - \boldsymbol{q}_{\mathrm{t}}$ satisfies

$$\ddot{\boldsymbol{e}}_{\mathrm{t}} + \mathbf{K}_1\dot{\boldsymbol{e}}_{\mathbf{t}} + \mathbf{K}_2\boldsymbol{e}_{\mathrm{t}} = \boldsymbol{f} + \boldsymbol{f}_1 \tag{39}$$

where $\boldsymbol{f}_1 = \ddot{\boldsymbol{x}}_1 + \mathbf{K}_1\dot{\boldsymbol{x}}_1 + \mathbf{K}_2\boldsymbol{x}_1 - \ddot{\boldsymbol{x}}_{\mathrm{h}} - \mathbf{K}_1\dot{\boldsymbol{x}}_{\mathrm{h}} - \mathbf{K}_2\boldsymbol{x}_{\mathrm{h}}$. Then $\ddot{\boldsymbol{x}}_1$ is

$$\ddot{\boldsymbol{x}}_1 = \ddot{\boldsymbol{q}}_{\mathrm{r}} = \boldsymbol{f} + \boldsymbol{f}_1 - \mathbf{K}_1\dot{\boldsymbol{e}}_{\mathrm{t}} - \mathbf{K}_2\boldsymbol{e}_{\mathrm{t}} + \ddot{\boldsymbol{q}}_{\mathrm{t}} \tag{40}$$

By Eq. (15) the flexible subsystem dynamic equation is

$$\mathbf{D}_{\mathrm{fr}}\ddot{\boldsymbol{q}}_{\mathrm{r}} + \mathbf{D}_{\mathrm{ff}}\ddot{\boldsymbol{q}}_{\mathrm{f}} + \boldsymbol{h}_{\mathrm{f}} + \mathbf{K}_{\mathrm{f}}\boldsymbol{q}_{\mathrm{f}} = \mathbf{0} \tag{41}$$

where $\boldsymbol{h}_{\mathrm{f}} = \mathbf{H}_{\mathrm{fr}}\dot{\boldsymbol{q}}_{\mathbf{r}} + \mathbf{H}_{\mathbf{ff}}\dot{\boldsymbol{q}}_{\mathrm{f}}$. By Eq. (40), the above flexible subsystem dynamic equation is transformed into

$$\ddot{\boldsymbol{q}}_{\mathrm{f}} = -\mathbf{D}_{\mathbf{ff}}^{-1}\mathbf{K}_{\mathrm{f}}\,\boldsymbol{q}_{\mathrm{f}} + \mathbf{D}_{\mathrm{ff}}^{-1}\mathbf{D}_{\mathrm{fr}}\left(\mathbf{K}_1\dot{\boldsymbol{e}}_{\mathrm{t}} + \mathbf{K}_2\mathbf{e}_{\mathrm{t}}\right) - \mathbf{D}_{\mathrm{ff}}^{-1}\mathbf{D}_{\mathrm{fr}}\boldsymbol{f} - \mathbf{D}_{\mathrm{ff}}^{-1}\left(\boldsymbol{h}_{\mathrm{f}} + \mathrm{D}_{\mathrm{fr}}\boldsymbol{f}_1\right) \tag{42}$$

By Eqs. (39) and (42), the Eq. (43) is derived

$$\dot{\boldsymbol{r}} = \mathbf{A}\boldsymbol{r} + \mathbf{B}\boldsymbol{f} + \boldsymbol{d} \tag{43}$$

https://doi.org/10.1017/S0263574719000857 Published online by Cambridge University Press

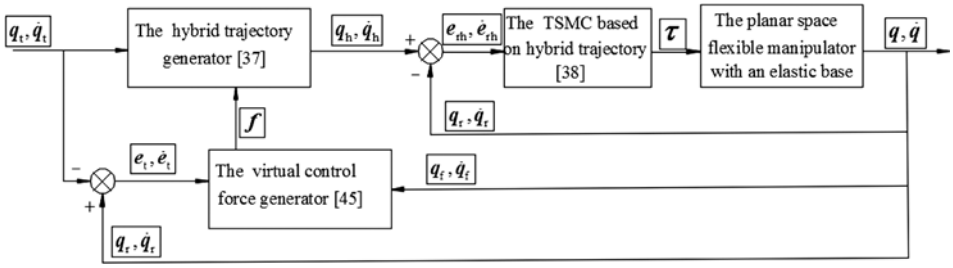


Fig. 3. The operational control strategy of the proposed TSMC based on hybrid trajectory.

where $\boldsymbol{r} = \left[\boldsymbol{q}_{\mathrm{f}}^{\mathrm{T}}\ \boldsymbol{e}_{\mathrm{t}}^{\mathrm{T}}\ \dot{\boldsymbol{q}}_{\mathrm{f}}^{\mathrm{T}}\ \dot{\boldsymbol{e}}_{\mathrm{t}}^{\mathrm{T}}\right]^{\mathrm{T}}$, $\mathbf{B} = \begin{pmatrix} \mathbf{0} \\ \mathbf{0} \\ -\mathbf{D}_{\mathrm{ff}}^{-1}\mathrm{D}_{\mathrm{fr}} \\ \mathrm{I} \end{pmatrix}$, $\boldsymbol{d} = \begin{pmatrix} \mathbf{0} \\ \mathbf{0} \\ -\mathbf{D}_{\mathrm{ff}}^{-1}\left(\boldsymbol{h}_{\mathrm{f}} + \mathbf{D}_{\mathrm{fr}}\boldsymbol{f}_1\right) \\ \boldsymbol{f}_1 \end{pmatrix}$,

$\mathbf{A} = \begin{pmatrix} \mathbf{0} & \mathbf{0} & \mathbf{I} & \mathbf{0} \\ \mathbf{0} & \mathbf{0} & \mathbf{0} & \mathbf{I} \\ -\mathbf{D}_{\mathrm{ff}}^{-1}\mathbf{K}_{\mathrm{f}} & \mathbf{D}_{\mathrm{ff}}^{-1}\mathbf{D}_{\mathrm{fr}}\mathbf{K}_2 & \mathbf{0} & \mathbf{D}_{\mathrm{ff}}^{-1}\mathbf{D}_{\mathrm{fr}}\mathbf{K}_1 \\ \mathbf{0} & -\mathbf{K}_2 & \mathbf{0} & -\mathbf{K}_1 \end{pmatrix}$,

$\boldsymbol{d}$ may be considered as external disturbances. To minimize the flexible vibration, the virtual control force and the actual error simultaneously, the following optimal cost function is chosen

$$J = \frac{1}{2}\int_0^{\infty} (\boldsymbol{r}^{\mathrm{T}}\mathbf{Q}_1\boldsymbol{r} + \boldsymbol{f}^{\mathrm{T}}\mathbf{Q}_2\boldsymbol{f})\mathrm{d}t \tag{44}$$

where $\mathbf{Q}_1$ and $\mathbf{Q}_2$ are the weighting matrices of the state vector $\boldsymbol{r}$ and the virtual control force $\boldsymbol{f}$, respectively. So, the virtual control force $\boldsymbol{f}$ is

$$\boldsymbol{f} = -\mathbf{K}_{opt}\,\boldsymbol{r}(t) = -\mathbf{Q}_2^{-1}\mathbf{B}^{\mathrm{T}}\mathbf{G}\boldsymbol{r}(t) \tag{45}$$

where $\mathbf{G}$ is the solution of the following Ricatti equation

$$\mathbf{G}\mathbf{A} + \mathbf{A}^{\mathrm{T}}\mathbf{G} - \mathbf{G}\mathbf{B}\mathbf{Q}_2^{-1}\mathbf{B}^{\mathrm{T}}\mathbf{G} + \mathbf{Q}_1 = \mathbf{0} \tag{46}$$

Then Eq. (43) is transformed into

$$\dot{\boldsymbol{r}} = (\mathbf{A} - \mathbf{B}\mathbf{Q}_2^{-1}\mathbf{B}^{\mathrm{T}}\mathbf{G})\boldsymbol{r} + \boldsymbol{d} \tag{47}$$

When $\boldsymbol{d} = \mathbf{0}$, the optimal controller Eq. (45) can ensure the system Eq. (43) asymptotically stable. When $\boldsymbol{d} \neq \mathbf{0}$, let $\mathbf{N}_1 = \mathbf{Q}_1 + \mathbf{A}^{\mathrm{T}}\mathbf{G}$ and introduce the Lyapunov function V_1

$$V_1 = \boldsymbol{r}^{\mathrm{T}}\boldsymbol{r} \tag{48}$$

Then the derivative of V_1 is

$$\dot{V}_1 = 2\boldsymbol{r}^{\mathrm{T}}\dot{\boldsymbol{r}} = 2\boldsymbol{r}^{\mathrm{T}}\left(\left(-\mathbf{G}^{-1}\mathbf{N}_1\right)\boldsymbol{r} + \boldsymbol{d}\right) \tag{49}$$

If the Eq. (50) is ensured

$$\frac{\|\boldsymbol{d}\|}{\|\boldsymbol{r}\|} \leq \mu = \lambda_{\min}\left(\mathbf{G}^{-1}\mathbf{N}_1\right) = \frac{N_{1\,\min}}{G_{\max}} \tag{50}$$

$\dot{V}_1 \leq 0$, $\lim_{t\to\infty} \boldsymbol{r} = \mathbf{0}$, the closed system Eq. (43) is to be asymptotically stable.

Therefore the hybrid trajectory based controller Eq. (38) can asymptotically track the terminal trajectory $\boldsymbol{q}_{\mathrm{t}}$ with the link flexible vibrations and the elastic base deformation are well damped out.

The operational control strategy of the proposed TSMC based on hybrid trajectory is shown in Fig. 3.

https://doi.org/10.1017/S0263574719000857 Published online by Cambridge University Press

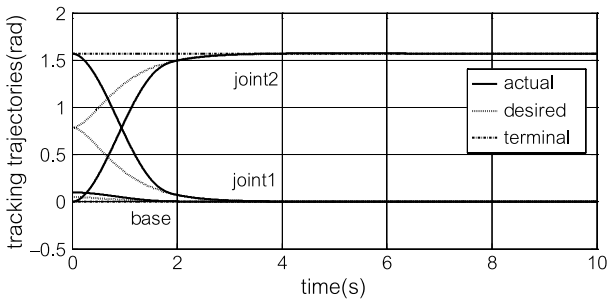


Fig. 4. The tracking trajectories of the base's attitude and joints' angle (TSMC based on desired trajectory).

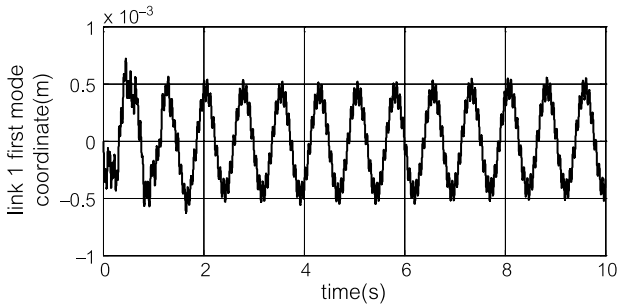


Fig. 5. The first vibration mode coordinate of link 1 (TSMC based on desired trajectory).

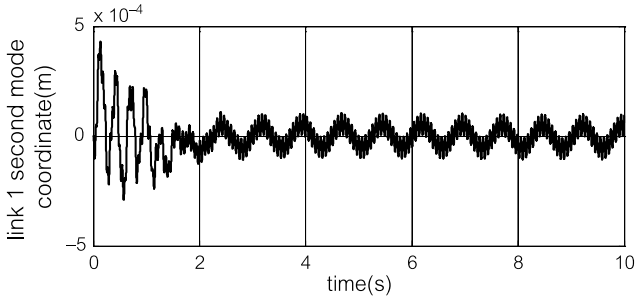


Fig. 6. The second vibration mode coordinate of link 1 (TSMC based on desired trajectory).

5. Simulation Examples

To show the performance of the proposed controller, simulations are carried out on a planar space manipulator system shown in Fig. 1. The actual parameters of the system are as follows: $l_0 = l_2 = 1.0\,\text{m}$, $l_1 = 2.0\,\text{m}$, $m_0 = 200\,\text{kg}$, $\rho_1 = 4\,\text{kg/m}$, $\rho_2 = 1.6\,\text{kg/m}$, $m_{\text{a1}} = m_{\text{a2}} = 1\,\text{kg}$, $m_P = 14.4\,\text{kg}$, $I_0 = 100\,\text{kg}\cdot\text{m}^2$, $I_P = 41.7\,\text{kg}\cdot\text{m}^2$, $(EI)_1 = 500\,N.m^2$, $(EI)_2 = 300\,N.m^2$, $I_{\text{a1}} = I_{\text{a2}} = 0.03kg\,m^2$, $k = 5000\,N/\text{m}$, $\boldsymbol{\tau}_{\text{d}} = 10 \times [\sin(0.25\pi t)\cos(0.25\pi t)\sin(0.25\pi t) - \cos(0.25\pi t)]^{\text{T}}$.

The terminal angle vector is defined as $\boldsymbol{q}_{\text{t}} = [000.5\pi]^{\text{T}}$. The initial state of the space manipulator is $\Delta l_0 = \delta_{11}(0) = \delta_{12}(0) = \delta_{21}(0) = \delta_{22}(0) = 0\,m$, $\theta_0(0) = 0.1$ rad, $\theta_1(0) = 0.5\pi\,rad$, $\theta_2(0) = 0$. The control parameters are $\boldsymbol{Z}_1 = diag([2, 10, 10])$, $\boldsymbol{Z}_2 = diag([15, 60, 60])$, $c = 80$, $c_0 = 60$, $c_1 = 20$, $\boldsymbol{K}_1 = diag([4, 4, 4])$, $\boldsymbol{K}_2 = diag([4, 4, 4])$, $\boldsymbol{Q}_1 = diag([1, 30, 5, 300, 1, 1, 1, 1, 1, 30, 5, 300, 1, 1, 1, 1])$, $\boldsymbol{Q}_2 = diag([0.1, 0.1, 0.1])$. The time taking in the simulation is $t = 10\,\text{s}$.

The simulation results from TSMC based on desired trajectory Eq. (23) are shown in Figs. 4–10. The tracking trajectories are depicted in Fig. 4. Figures 5 and 6 are the first and the second vibration mode coordinate of the flexible link 1. Figures 7 and 8 are the first and the second vibration mode coordinate of the flexible link 2. Figure 9 is the base's deformation. The input torques are shown in Fig. 10.

The simulation results from TSMC based on hybrid trajectory Eq. (38) are shown in Figs. 11–19. The base's attitude trajectories are depicted in Fig. 11. Figure 12 shows the angular trajectories of joint 1 and Fig. 13 shows the angular trajectories of joint 2. Figures 14 and 15 are the first and the

https://doi.org/10.1017/S0263574719000857 Published online by Cambridge University Press

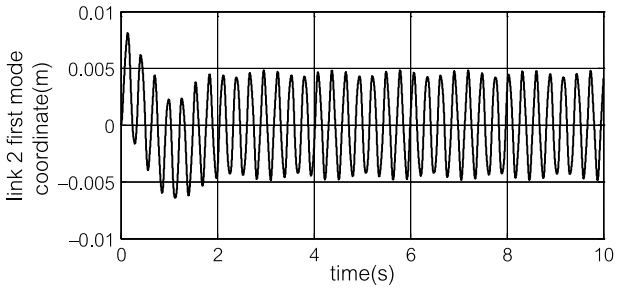


Fig. 7. The first vibration mode coordinate of link 2 (TSMC based on desired trajectory).

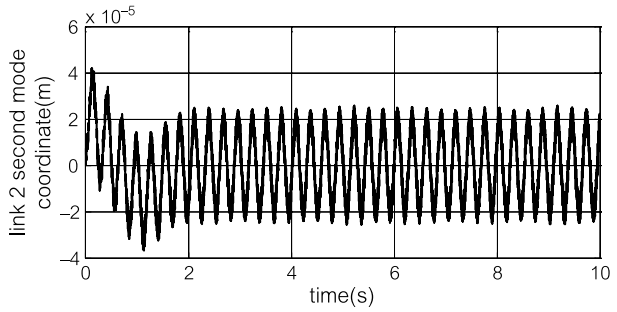


Fig. 8. The second vibration mode coordinate of link 2 (TSMC based on desired trajectory).

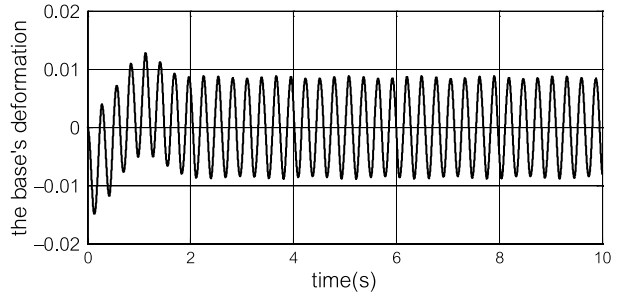


Fig. 9. The base's deformation (TSMC based on desired trajectory)

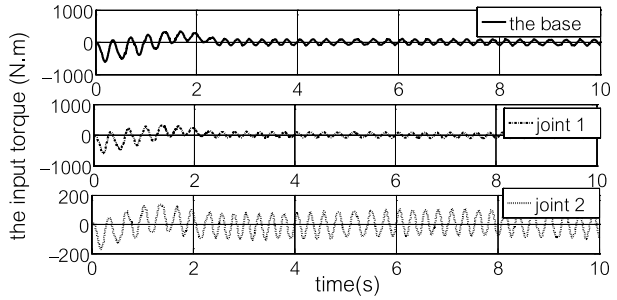


Fig. 10. The input torques (TSMC based on desired trajectory).

second vibration mode coordinate of the flexible link 1. Figures 16 and 17 are the first vibration mode coordinate of the flexible link 2. Figure 18 is the base's deformation. The input torques are shown in Fig. 19.

The simulation results show that the actual angle vector $\boldsymbol{q}_r$ both asymptotically track the terminal angle vector q_t under the two controllers. (By TSMC based on desired trajectory, the ultimate angular errors of the base's attitude, the joint 1 and the joint 2 are 0.0009, 0.0006, 0.004 rad, respectively. By TSMC based on hybrid trajectory, the ultimate angular errors of the base's attitude, the joint

https://doi.org/10.1017/S0263574719000857 Published online by Cambridge University Press

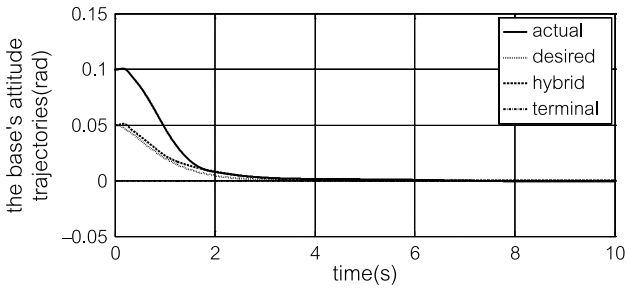


Fig. 11. The base's attitude trajectories (TSMC based on hybrid trajectory).

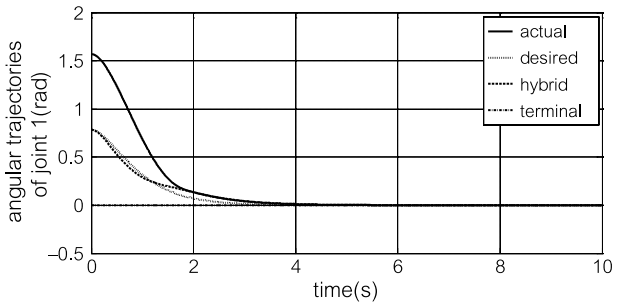


Fig. 12. The angular trajectories of joint 1 (TSMC based on hybrid trajectory).

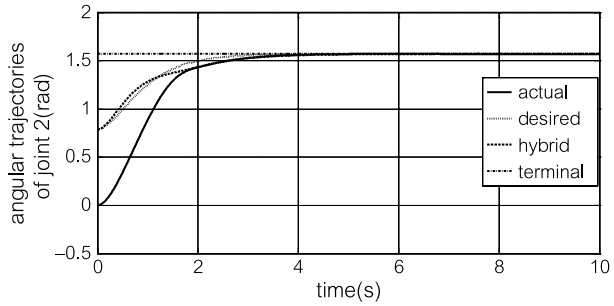


Fig. 13. The angular trajectories of joint 2 (TSMC based on hybrid trajectory).

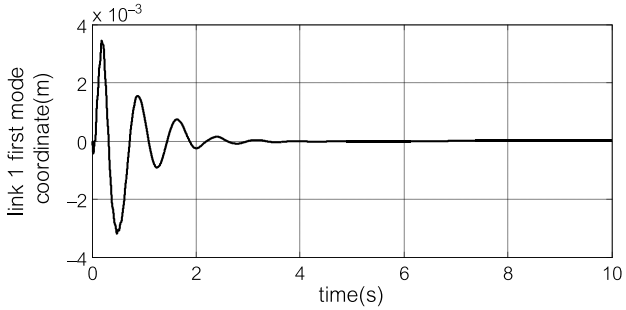


Fig. 14. The first vibration mode coordinate of link 1 (TSMC based on hybrid trajectory).

1 and the joint 2 are 0.0006, 0.0004, 0.002 rad, respectively.) The base's elastic deformation, the first and second mode vibration coordination are asymptotically stable under the TSMC based on hybrid trajectory, nevertheless, the base's elastic deformation, the first and second mode vibration coordination fluctuate back and forth in a relatively large range all the time under the TSMC based on desired trajectory. The input torques based on the two controllers are almost the same at the start (probably before 0.25 s); however, the input torques of TSMC based on the hybrid trajectory are obviously lower than those of TSMC based on the desired trajectory 0.25 s later.

https://doi.org/10.1017/S0263574719000857 Published online by Cambridge University Press

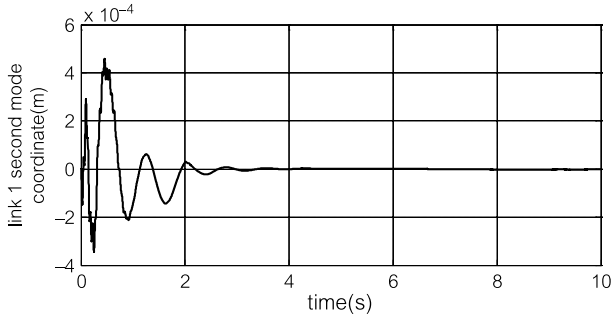


Fig. 15. The second vibration mode coordinate of link 1 (TSMC based on hybrid trajectory).

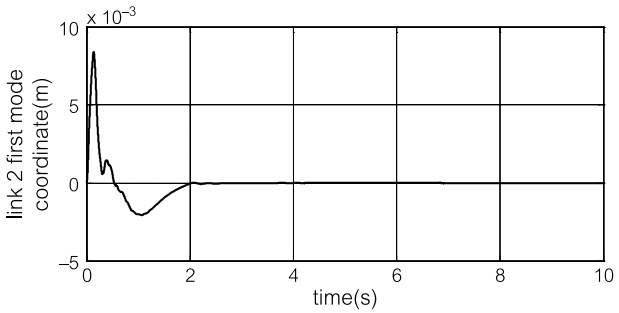


Fig. 16. The first vibration mode coordinate of link 2 (TSMC based on hybrid trajectory).

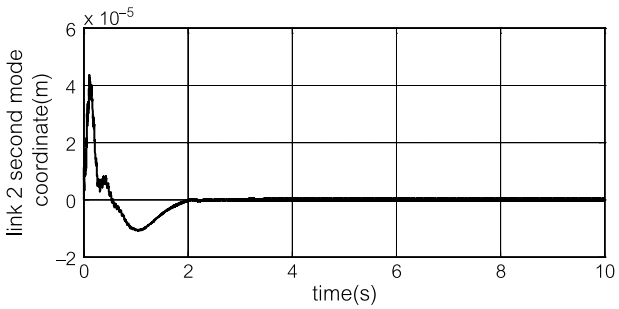


Fig. 17. The second vibration mode coordinate of link 2 (TSMC based on hybrid trajectory).

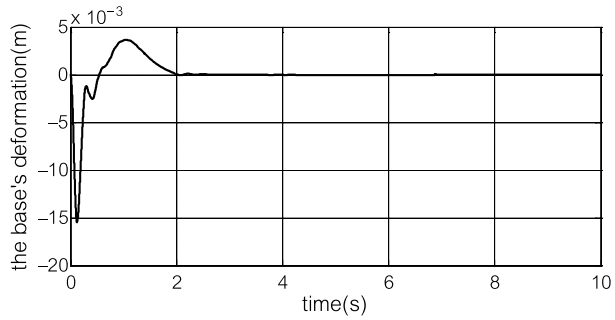


Fig. 18. The base's deformation (TSMC based on hybrid trajectory).

6. Conclusions

The dynamic model of a free-flying space manipulator with two flexible links and an elastic base was derived from the Lagrange equations, assumed mode technique and linear momentum conservation theory. A TSMC based on desired trajectory was proposed to control the free-flying space manipulator while parametric uncertainties and modeling errors exist. This controller asymptotically

https://doi.org/10.1017/S0263574719000857 Published online by Cambridge University Press

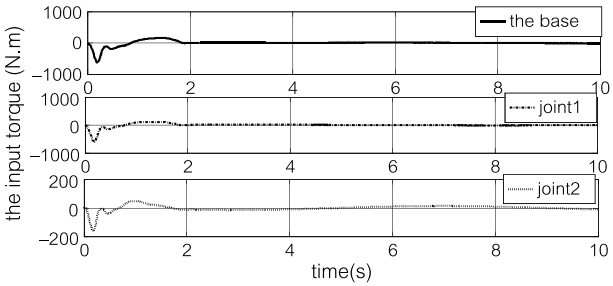


Fig. 19. The input torques (TSMC based on hybrid trajectory).

tracked the terminal trajectory, nevertheless the flexible dynamics remained unstable. Furthermore, a TSMC based on hybrid trajectory was proposed, in which the hybrid trajectory was generated from the virtual control force concept and the terminal trajectory. This controller assured the flexible vibrations of the space manipulator were stabilized effectively with good tracking performance. The two proposed controllers can be extended to space manipulator with elastic base and arbitrary flexible arms.

Acknowledgments

This work was supported by the National Natural Science Foundation of China (No. 51741502, No. 11372073, No. 61673115), Fujian Provincial Industrial Robot Basic Components' Technology Research Platform (No.2014H21010011) and the Natural Science Foundation of Fujian Province (No. 2016J01228).

References

1. R. Boumans and C. Heemskerk, "The European robotic arm for the International Space Station," *Robot. Auton. Syst.* **23**(1), 17–27 (1998).
2. M. Garneau, "Space in the Service of Society: A Canadian Case Study," *Proceedings of 2nd International Conference on Recent Advances in Space Technologies*, Istanbul, Turkey (2005), pp. 1–6.
3. M. Nohmi, "Development of Space Tethered Autonomous Robotic Satellite," *Proceedings of 3rd International Conference on Recent Advances in Space Technologies*, Istanbul, Turkey (2007) pp. 462–467.
4. L. B. Holcomb and M. D. Montemerlo, "NASA automation and robotics technology program," *IEEE Aerosp. Electron. Syst. Mag.* **2**(4), 19–26 (2009).
5. K. Yoshida, "Achievements in space robotics," *IEEE Robot. Autom. Mag.* **16**(4), 20–28 (2009).
6. M. W. Walker and L. B. Wee, "Adaptive control of space-based robot manipulators," *IEEE Trans. Robot. Autom.* **7**(6), 828–835 (1991).
7. Y. L. Gu and Y. Xu, "A normal form augmentation approach to adaptive control of space robot systems," *Dyn. Control* **5**(3), 275–294 (1995).
8. O. Parlaktuna and M. Ozkan, "Adaptive control of free-floating space robots in Cartesian coordinates," *Adv. Robot.* **18**(9), 943–959 (2004).
9. R. M. Sanner and E. E. Vance, "Adaptive Control of Free-Floating Space Robots Using Neural Networks," *Proceedings of the 1995 American Control Conference*, Seattle, WA (1995) pp. 2790–2794.
10. T. de FPA Taveira, A. A. Siqueira and H. Terra, "Adaptive Nonlinear H8 Controllers Applied to a Free-Floating Space Manipulator," *Proceedings of the 2006 IEEE International Conference on Control Applications*, Munich, Germany (2006) pp. 1476–1481.
11. A. Flores-Abad and O. Ma, "Control of a Space Robot for Minimal Attitude Disturbance to the Base Satellite for Capturing a Tumbling Satellite," *Proceedings of SPIE Sensors and Systems for Space Applications V*, Baltimore, USA, vol. 8385 (2012).
12. L. CH. Wu, F. CH. Sun, Z. Q. Sun and W. J. Su, "Dynamic Modeling, Control and Simulation of Flexible Dual-Arm Space Robot," *Proceedings of 2002 IEEE Region 10 Conference on Computers, Communications, Control and Power*, Beijing, China (2002) pp. 1282–1285.
13. K. Senda and Y. Murotsu, "Methodology for control of a space robot with flexible links," *IEEE Proc. Control Theory Appl.* **47**(6), 562–568 (2000).
14. J. Carusone, K. S. Buchan and G. M. T. D'Eleuterio, "Experiments in end-effector tracking control for structurally flexible space manipulators," *IEEE Trans. Robot. Autom.* **9**(5), 553–560 (1993).
15. ZH. B. Hong and L. Chen, "Active vibration control and fuzzy control of free-floating space flexible manipulator based on singular perturbation theory," *J. Mech. Eng.* **46**(7), 35–41 (2010).
16. Y. Murotsu, S. Tsujio, K. Senda and M. Hayashi, "Trajectory control of flexible manipulators on a free-flying space robot," *IEEE Control Syst. Mag.* **12**(3), 51–57 (1992).
17. J. Liang and L. Chen, "Fuzzy logic adaptive compensation control of end-effect motion and flexible vibration for space-based flexible manipulator," *Acta ArmamentarII* **32**(1), 45–57 (2011).

https://doi.org/10.1017/S0263574719000857 Published online by Cambridge University Press

18. X. Y. Yu and L. Chen, "Singular perturbation adaptive control and vibration suppression of free-flying flexible space manipulators," *Proc. IMechE Part C: J. Mech. Eng. Sci.* **229**(11), 1989–1997 (2015).
19. L. D. Akulenko, S. S. Krylov, G. Markov Yu, T. T. Win and A. S. Filippova, "Dynamics of spacecraft with elastic and dissipative elements in the attitude control mode," *J. Comput. Syst. Sci. Int.* **53**(5), 723–732 (2014).
20. X. T. Tran and H. J. Kang, "Adaptive hybrid high-order terminal sliding mode control of MIMO uncertain nonlinear systems and application to robot manipulators," *Int. J. Precis. Eng. Manuf.* **16**(2), 255–266 (2015).
21. S. Ding, J. Wang and W. X. Zheng, "Second-order sliding mode control for nonlinear uncertain systems bounded by positive functions," *IEEE Trans. Ind. Electron.* **62**(9), 5899–5909 (2015).
22. A. Nasiri, S. Kiong Nguang and A. Swain, "Adaptive sliding mode control for a class of MIMO nonlinear systems with uncertainties," *J. Franklin Inst. B* **351**(4), 2048–2061 (2014).
23. H. Alwi and C. Edwards, "Sliding mode fault-tolerant control of an octorotor using linear parameter varying-based schemes," *IET Control Theory Appl.* **9**(4), 618–636 (2015).
24. R. Su and Q. Zong, "Comprehensive design of disturbance observer and non-singular terminal sliding," *IET Control Theory Appl.* **9**(12), 1821–1830 (2015).
25. A. Al-Ghanimi, Z. Man and J. Zheng, "Robust and fast non-singular terminal sliding mode control for piezoelectric actuators," *IET Control Theory Appl.* **9**(18), 2678–2687 (2015).
26. Y. S. Guo and L. Chen, "Terminal sliding mode control for coordinated motion of a space rigid manipulator with external disturbance," *Appl. Math. Mech.* **29**(5), 583–590 (2008).
27. A. De Luca and B. Siciliano, "Closed-form dynamic model of planar multilink lightweight robots," *IEEE Trans. Syst. Man Cybern.* **21**(4), 826–839 (1991).
28. X. Y. Yu and L. Chen, "Robust Motion Control and Vibration Optimal Control for a Free-Flying Flexible Space Manipulator with Elastic Base," *Proceedings of the the 67th International Astronautical Congress*, Guadalajala, Mexico (2016).
29. R. P. Signh, R. J. Vandervoort and P. W. Likins, "Dynamics of flexible bodies in tree topology – a computer oriented approach," *J. Guid. Control Dyn.* **8**, 584–590 (1985).

https://doi.org/10.1017/S0263574719000857 Published online by Cambridge University Press